Journal of Materials Chemistry

Cite this: *J. Mater. Chem.*, 2011, **21**, 5660

www.rsc.org/materials

PAPER

Preparation and characterization of temperature-responsive and magnetic nanomicelles

Chi Huang,[a] Yangbo Zhou,[b] Yong Jin,[c] Xiaofeng Zhou,[c] Zhaomin Tang,[b] Xing Guo[b] and Shaobing Zhou*[ab]

Received 7th December 2010, Accepted 14th February 2011
DOI: 10.1039/c0jm04264a

One type of the temperature-responsive and magnetic nanomicelles was synthesized based on SPIONs (superparamagnetic iron oxide nanoparticles) and the biocompatible polymer-Pluronic F127 or its copolymer with poly(DL-lactic acid) (F127–PLA) *via* a facile chemical conjugation method. The magnetic nanomicelles were characterized by Fourier transform infrared spectroscopy (FT-IR), X-ray powder diffraction (XRD), thermogravimetric analysis (TGA), a vibrating sample magnetometer (VSM), dynamic light scattering measurements (DLS), transmission electron microscopy (TEM) and atomic force microscopy (AFM). The varying volume shrinkage of the magnetic nanomicelles was detected when increasing the temperature from 15 to 45 °C. Doxorubicin hydrochloride (DOX·HCl) was selected as a model anticancer drug to investigate the drug loading and release behavior in the buffer solutions with different pH values and in an alternating magnetic field (MF). The Alamar blue assay was performed to evaluate the biocompatibility of the micelles and the antiproliferative effect of the drug-loaded micelles. The results displayed that the magnetic micelles were safe carriers and the DOX·HCl-loaded micelles were equally effective as the free drug for suppressing the growth of tumor cells. The blood compatibility studies showed few effects on coagulation and hemolysis. Therefore, the magnetic micelles possess many great potential applications in the field of nanomedicine.

1. Introduction

Superparamagnetic iron oxide nanoparticles (SPIONs) have been extensively studied in the fields of biomolecular separation, magnetic resonance imaging, magnetic drug delivery and cancer treatment. Due to being quite benign toward humans, SPIONs are approved by the US food and drug administration (FDA).[1–3] However, primary SPIONs aggregate as a result of their large surface energy and the interaction between dipoles. When they aggregate in the body, they are quickly cleared by macrophages or are accumulated in the reticule-endothelial system (RES).[4,5] An approach to solving this problem is to modify the SPIONs' surface with biocompatible polymers. These modified SPIONs could provide an efficient system to prolong the particulate circulation time in blood, additionally, they could also provide an active functional group for conjugation with the targeting ligands, drugs and fluorescent dyes, which could broaden their biomedical applications.[5,6] To date, several modifications including the physical adsorption method[7,8] and the chemical conjugation method[5,9] have been developed to tailor the SPIONs. In the former method, the SPIONs are coated with ligands by means of either electrostatic or hydrophobic interactions during the synthesis. This method is very flexible and effective, nevertheless, it tends to form larger clusters due to aggregation and precipitation under physiological conditions.[10] The chemical conjugation method usually requires a coupling agent to make a bridge between the SPIONs and the ligands. Therefore, modified SPIONs with a smaller size are stable in various external environments due to the covalent linkages.

Formulation of the magnetic nanomicelles can be realized by using the various FDA-approved biocompatible polymers such as PLA and pluronic copolymers. Pluronic copolymers not only exhibit temperature-responsive behavior, but can also cross many impermeable barriers such as the blood-brain barrier and thus can overcome the multiple drug resistance phenomena in cancer therapy.[7,11] They are composed of poly(ethylene oxide)-*block*-poly(propylene oxide)-*block*-poly(ethylene oxide) (PEO–PPO–PEO). Triggered by a temperature change, pluronics will self-assemble into a micelle with a hydrophobic PPO core, which serves as a microenvironment for incorporating the lipophilic drug, and with a coronal shell formed by PEO, which enhances the stability and longevity of the drug carriers in blood at around body temperature.[11,12] Additionally, PLA, as a biodegradable

[a]*School of Materials Science and Engineering, Key Laboratory of Advanced Technologies of Materials, Ministry of Education, Southwest Jiaotong University, Chengdu, 610031, P. R. China. E-mail: shaobingzhou@swjtu.edu.cn; shaobingzhou@hotmail.com; Fax: +86 2887634649; Tel: +86 2887634023*
[b]*School of Life Science and Engineering, Southwest Jiaotong University, Chengdou, 610031, Sichuan, P. R. China*
[c]*Interventional Therapy Department, The Second Affiliated Hospital, Soochow University, 215004 Suzhou, China*

polymer, can be degraded into natural metabolites, thereby decreasing the toxic effects in the body.[13] Meanwhile, the micelle size and morphology can be tuned using the hydrophobic PLA segments.

The design of the entirely new nanofabricated systems is required for targeting the local transportation of drug. Multifunctional nanomaterials have been demonstrated to be ideal candidates for targeted drug delivery. Herein, magnetic nanomicelles were fabricated and were investigated as the anticancer drug carriers. The micelles comprised of SPIONs chemically conjugated with temperature-responsive Pluronic F127 or F127–PLA. The principle is schematically illustrated in Fig. 1. Firstly, SPIONs coated with oleic acid (OA) were obtained by the classical chemical coprecipitation method. Later, the F127 and F127-PLA ligands were covalently grafted onto the SPIONs' surface by an NCO-functionalized silane coupling agent.

2. Experimental section

2.1 Materials

Ferrous chloride tetrahydrate ($FeCl_2 \cdot 4H_2O$), ferric chloride hexahydrate ($FeCl_3 \cdot 6H_2O$), aqueous ammonium hydroxide (NH_4OH, 25–28%, w/w), chloroform, toluene, NaCl, triethylamine (Et_3N) and oleic acid (OA) were purchased from Chengdu KeLong Chemical Reagent Company (Sichuan, China) and used as received. 3-(Triethoxysily) propyl isocyanate (TPI) was purchased from Tokyo Chemical Industry Company (Tokyo, Japan) and used as received. Pluronic F127 (Mn 12 600) was purchased from Aldrich (USA) and used as received. Poly(DL-lactic acid) (PLA, Mn 600) was synthesized as our previous report.[14] Alamar blue cell viability reagent was purchased from Invitrogen (USA). DOX·HCl was purchased from Zhejiang Hisun Pharmaceutical (China). The HepG2 (human liver carcinoma cells) cells were purchased from the American Type Culture Collection (ATCC; Rockville, MD, USA). Fresh human blood was purchased from Chengdu Blood Center (Sichuan, China).

2.2 Synthesis of SPIONs

The SPIONs were prepared by the modified chemical co-precipitation method as described in our previous report.[15] In brief, 20 mmol $FeCl_3 \cdot 6H_2O$ and 10 mmol $FeCl_2 \cdot 4H_2O$ were dissolved in 100 mL distilled water. Then, 25 mL NH_4OH and 1 mL OA were added with vigorous stirring under the protection of a nitrogen atmosphere at 80 °C for 1 h.

After the reaction, these SPIONs were extracted into toluene by adding NaCl as an inducer. The toluene dispersion was refluxed to remove the residual water under a nitrogen atmosphere and the SPION dispersion was diluted with toluene to 40 mg mL^{-1} for further use.

2.3 Synthesis of F127 covalently grafted SPIONs (SPIONs@F127)

The synthesis of SPIONs@F127 was divided into two steps as shown in Fig. 1: (1) the F127–TPI ligands were prepared using an isocyanate-hydroxyl reaction. 0.1 mmol F127 was dissolved in 30 mL dried chloroform. Later, 0.1 mmol TPI was added, and

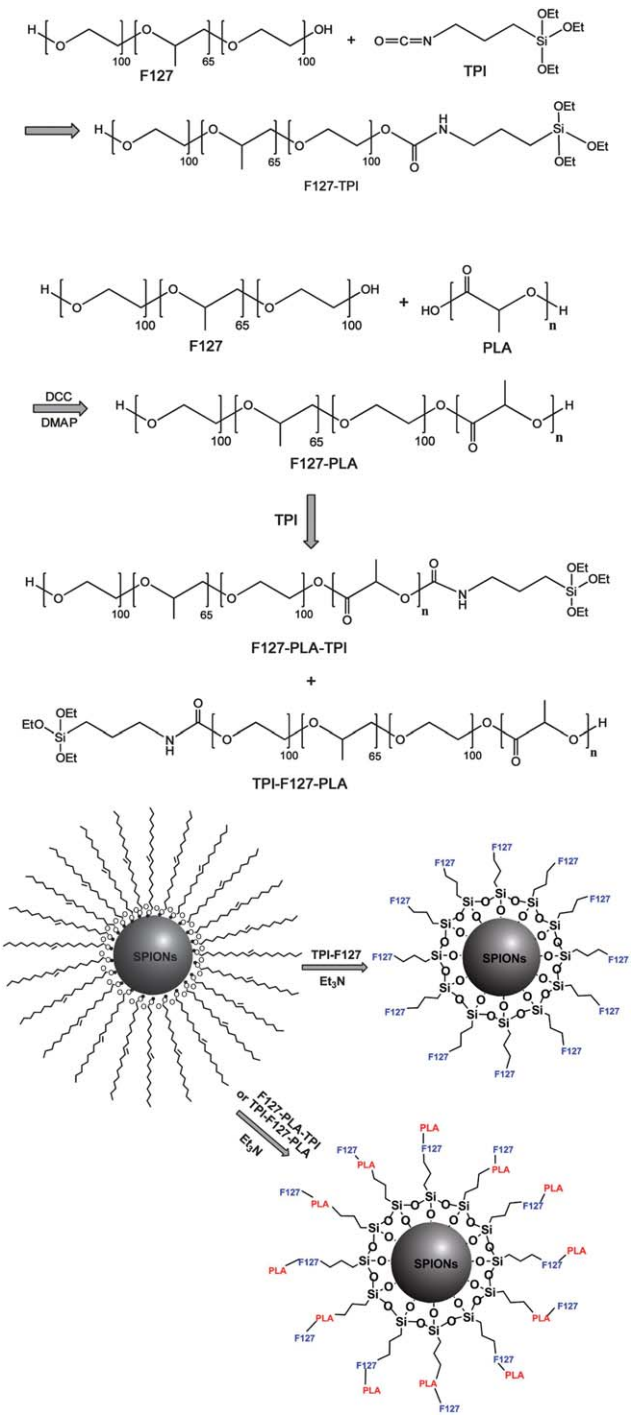

Fig. 1 Schematic illustration of chemical grafting of F127 and F127–PLA onto the surface of SPIONs.

the solution was stirred overnight under nitrogen; (2) 500 μL of the 40 mg mL^{-1} SPIONs dispersion and 10 μL of Et_3N were added dropwise into the F127–TPI solution, and the solution was stirred overnight under nitrogen. To prepare the magnetic nanomicelles, the SPIONs@F127 dispersion was dried in a vacuum oven and then resuspended in tetrahydrofuran by ultrasonication. Later, the complex solution was added dropwise into an aqueous phase and underwent ultrasonication for 8 h to form micelles. and finally the solution was poured into a dialysis

membrane (MWCO 14000) and dialyzed against distilled water for 3 days to remove the residual F127.[16] The aqueous solutions were freeze-dried and the resulting products were stored at −4 °C for further use.

2.4 Synthesis of F127–PLA covalently grafted SPIONs (SPIONs@F127-PLA)

The synthesis of SPIONs@F127–PLA was also divided into two steps. Firstly, the F127–PLA block copolymers were synthesized according to the literature.[17] The mixed solution containing 0.1 mmol PLA and 0.1 mmol F127 dissolved in 30 mL of dried chloroform was activated by adding both 0.12 mmol *N*,*N*′-dicyclohexyl-carbodiimide (DCC) and 4-dimethy-laminopyridine (DMAP). The mixture was stirred for 30 min at 0 °C and for another 12 h at ambient temperature. After filtration, 0.1 mmol TPI was added to the resultant solution, then stirred overnight under nitrogen. Secondly, 500 μL of the 40 mg mL^{-1} SPION toluene dispersion and 10 μL of Et_3N were added dropwise into the F127–PLA solution. The following procedure was similar to the fabrication of SPIONs@F127 referred above.

2.5 Synthesis of F127 physical adsorbed SPIONs (SPIONs–F127)

The synthesis of F127–SPIONs by use of the physical adsorbing method was carried out according to the literature.[16] 500 μL of the SPION toluene dispersion was added to 30 mL F127 (0.1 mmol) chloroform solution and the solution was stirred overnight under nitrogen. The following procedure was similar to the fabrication of SPIONs@F127 above.

2.6 Characterization

FT-IR (Nicolet 5700) was performed to analyze the surface functionalization of the SPIONs. The modified nanoparticles were analyzed for phase composition with XRD (Philips X'Pert PRO) over the 2θ range from 20–90° at rate of 2.5° min^{-1}, using Cu-Kα radiation ($\lambda = 1.54060$ Å) at ambient temperature. TGA was performed on a TA instrument (Netzsch STA 449C, Bavaria, Germany) at a scan rate of 10 °C min^{-1}, up to 700 °C under a nitrogen atmosphere. The magnetic properties were measured with a VSM (Quantum Design) at ambient temperature. The morphology and size were observed by TEM (HITACHI H-700H) at an accelerating voltage of 175 kV and AFM (CSPM5000, Being, China). Particle size and its distribution were determined by a Particle Size Analyzer (ZETA-SIZER, MALVERN Nano-ZS90). The maximum loading amount of DOX·HCl in the magnetic nanomicelles was determined by Fluoromax spectrometer (F-7000, HITACH, Japan) at an excitation 370 nm and emission recorded in the interval of 500–700 nm. The qualitative proof and the stability of SPIONs@F127 and SPIONs@F127–PLA micelles were determined by UV-visible spectrophotometry (UV-2550, Shimadzu, Japan), and the absorbance at 273 nm was measured to determine the concentration of DOX·HCl released.

2.7 Drug loading and *in vitro* release

The maximum loading amount of DOX·HCl was determined by the serial addition of the magnetic nanomicelles to the DOX·HCl solution. Increasing amounts of magnetic nanomicelles were dispersed in the DOX·HCl tetrahydrofuran solution (0.1 mg DOX·HCl in 2 mL tetrahydrofuran), then the complex solution was added dropwise to 3 mL PBS and ultrasonicated for 8 h, and the mixture were freeze-dried and stored at −4 °C before any measurement. Finally, those samples were resuspended in 3 mL PBS and the corresponding fluorescence was monitored. The fluorescence of DOX·HCl was quenched when the compounds were adsorbed into the micelles.[18–20]

The *in vitro* drug release from the magnetic nanomicelles was studied by using a dialysis membrane (MWCO 14000) in an acetate buffered solution (ABS, pH 5.1) and a phosphate buffered solution (PBS, pH 7.4) with and without a MF (20 kHz and 15 kW)[21,22] respectively. All the drug release behaviors were carried out at 37 °C with a gentle shake over 140 h, but before the original 1.5, 4.5, 6.5, and 72.5 h, a MF stimulus was introduced over 10 min for the release behavior in PBS with MF. The DOX·HCl-loaded magnetic nanomicelles were transferred to a dialysis membrane and immersed in 20 mL PBS and ABS separately at 37 °C accompanied by a gentle shake. At appropriate intervals, 1.0 mL release medium was collected and 1.0 mL fresh buffer solution was added to the solution. The amount of DOX·HCl release was determined by a UV–visible spectrophotometer.

2.8 Cytotoxicity and histochemistry analysis

HepG2 cells were cultured in an RPMI 1640 medium supplemented with 10% fetal bovine serum (FBS) at 37 °C in a 5% CO_2 incubator. For the cytotoxicity test, HepG2 cells were seeded in 24-well tissue culture plates at a density of 1×10^4 cells per well in the medium. After 24 h, the culture media were replaced with 1.5 mL medium containing the various concentrations of SPIONS and the magnetic nanomicelles. The Alamar blue assay was performed after a culture period of 1, 2 and 3 days. To each well was added 280 μL Medium 199 (Ml99), 10 μL FBS, and 10 μL Alamar blue agent. After 4 hours the absorbance of the medium was read at 570 nm (mQ × 200, BIO–TEK, USA) against a medium-blank with Alamar blue agent. The difference of the absorbance between $E_{570\ nm,\ cells}$ and $E_{570\ nm,'blank}$ was linear with the number and activity of the cells.[23,24]

Prussian blue staining was performed to reveal the presence of iron cations. After incubation with the samples at a concentration of 100 μg mL^{-1} for 6 h, the cells were fixed with 3% formaldehyde and washed with PBS, followed by incubation with 2% potassium ferrocyanide in 6% hydrochloric acid for 30 min. After washing, they were counterstained with a neutral red solution. The samples were then examined with an optical microscope.

2.9 Hemolytic analysis

Heparin was added into fresh human blood as an anticoagulant, and stored at 4 °C before the experiments. A series of the magnetic micelles with different concentrations were incubated with 200 μL human blood, containing 10 mL normal saline solution, for 1 h under vortexing at 37 °C, the negative control

(normal saline solution) and the positive control (ultrapure water) were also prepared. Following this, each sample was centrifuged at 3000 rpm for 15 min and the supernatant was determined by UV-visible spectrophotometry at 541 nm. Percent hemolysis (hemolysis %) was calculated by the formula described as:

$$\text{Hemolysis}\% = \frac{A\text{s} - A\text{neg}}{A\text{pos} - A\text{neg}} * 100\%$$

Where As, Aneg, Apos are the absorbance of the sample, the negative control and the positive control, respectively.[25]

2.10 Coagulation analysis

Plasma was isolated by centrifuging at 3000 rpm for 15 min. The activated partial thromboplastin time (APTT) was determined with coagulometer (clot-72, HOSIPITEX). Each sample was added into 400 μL plasma at 37 °C for 15 min before adding the coagulation reagents. Control experiments were also done. Each experiment was repeated three times.[26]

2.11 Antiproliferative activity and intracellular delivery of the drug-loaded magnetic nanomicelles

For the antiproliferative activity test, HepG2 cells were seeded at 5000 cells per well in 96-well plates and were allowed to attach for 48 h. The cells were treated either with the drug solution or the drug-loaded magnetic nanomicelles at different doses. The cell viability was determined by Alamar blue assay. For fluorescent microscope study, HepG2 cells were seeded in 24-well tissue culture plates at a density of 1×10^4 cells per well in the medium. The drug-loaded magnetic nanomicelles dispersed in the cell culture medium at drug concentrations of 2 μg mL^{-1} were added into the wells. After incubation with samples for 6 h, the cells were fixed with 3% formaldehyde and washed with PBS. The samples were then examined with a fluorescence microscope.

3. Results and discussion

3.1 Characterization of the magnetic nanomicelles

The surface modification of SPIONs is critical to impart biocompatibility both *in vitro* and *in vivo*. In this study, we developed a functionalized amphiphilic biocompatible ligand immobilization to the SPIONs surfaces. Additionally the SPIONs could form micelles as a result of the ligands self-assembly in the aqueous phase. The structure of the functionalized SPIONs was identified by FT-IR analysis. Fig. 2A clearly demonstrates the chemical conjugation of the different types of amphiphilic polymers on the SPIONs. In Fig. 2A (1) the peaks at 1630 cm^{-1} and 1574 cm^{-1} are related to the asymmetric and symmetric COO^- vibration of the chelating bidentate interaction between OA and Fe on the surface of the particles. In Fig. 2A (2), the peaks in the range 1250–1000 cm^{-1} were attributed to C–O–C stretching and $–CH_2–$ rocking vibrations in the PEO–PPO–PEO chains of F127.[27] In Fig. 2A (3), the peak at 1763 cm^{-1} is due to the ester band in SPIONs@F127–PLA. The peak at about 549 cm^{-1} is related to the vibration of Fe–O. In Fig. 2B, six diffraction peaks at 2 theta = 30.1°, 35.6°, 43.3°, 53.5°, 57.2°, 62.9° assigned as the characteristic peaks of standard Fe_3O_4 crystal plane according to JCPDS [85–1436] were observed ,[19,28] which indicated that each sample contained Fe_3O_4 crystals with a cubic spinel structure and the incorporation of the polymers onto the SPIONs did not influence the Fe_3O_4 crystallization. The crystallite size of the sample was 12 nm calculated using Debye–Scherrer equation ($D = K\lambda/\beta\cos\theta$)

To further verify the successful synthesis of SPIONs@F127 and SPIONs@F127–PLA, TGA analysis was also performed at each step of the synthesis, as shown in Fig. 2C. The curve of the OA-coated SPIONs showed a weight loss of about 10.49% (Fig. 2C (1)). The weight loss from 200 °C to 350 °C was attributed to the degradation of OA. After grafting F127, the TGA curve showed two weight loss stages. As shown in Fig. 2C (2), there was a weight loss of about 0.8% during the first stage below 100 °C due to the evaporation of the residual water. In the second stage between 200 °C and 370 °C, the total weight loss was about 33.28% due to the decomposition of F127. Similarly, the TGA curve of SPIONs@F127–PLA (Fig. 2C (3)) showed that there were two predominant weight loss steps (completed at 200 °C and 400 °C respectively). The weight loss of SPIONs@F127–PLA increased to 34.83%.

To characterize the magnetic properties, VSM was used to record the hysteresis loops of the SPIONs at 300 K (Fig. 2D). The saturation magnetization value of the SPIONs, SPIONs@F127 and SPIONs@F127–PLA were 61.76, 42.53 and 34.32 emu g^{-1} respectively. This reduction might result from noncollinear spins at the polymer chemically conjugated on the particle surface and a related effect such as surface disorder.[29,30] Additionally, no hysteresis curve was detected for all of the samples which indicated that the characteristic superparamagnetic behaviors could prevent the magnetic materials from aggregating and enabled them to redisperse rapidly when the external magnetic field was removed. Meanwhile, this level of magnetization and superparamagnetism were of central importance for biomedical applications.[31,32]

3.2 Particle distribution and morphology of the magnetic nanomicelles

SPIONs@F127 and SPIONs@F127–PLA could self-assemble into the magnetic nanomicelles in aqueous solution due to the hydrophobic forces. TEM and AFM were used to observe the morphology of the samples dispersed in the organic and aqueous phase, respectively. As seen from Fig. 3A, B and C, the SPIONs and the magnetic nanomicelles possessed good dispersity in chloroform, which indicated that OA, F127 and F127–PLA immobilized on the SPIONs could support the nanoparticles dispersion in the organic phase as a result of the steric repulsion forces. After the phase transformation, the particle size and morphology of the magnetic nanomicelles changed. The TEM photo (Fig. 3D) showed that SPIONs@F127 aggregated a little in the aqueous phase compared with the organic phase. However, SPIONs@F127–PLA aggregated spontaneously to form a few clusters (Fig. 3E). From the inset of Fig. 3E, the clusters were composed of the magnetic nanoparticles with a size of about 10 nm. A similar situation was observed in the AFM images (Fig. 3F, G), The clusters of SPIONs@F127–PLA with larger size were formed in the aqueous phase compared to SPIONs@F127. Fig. 3H and I displayed that in the organic

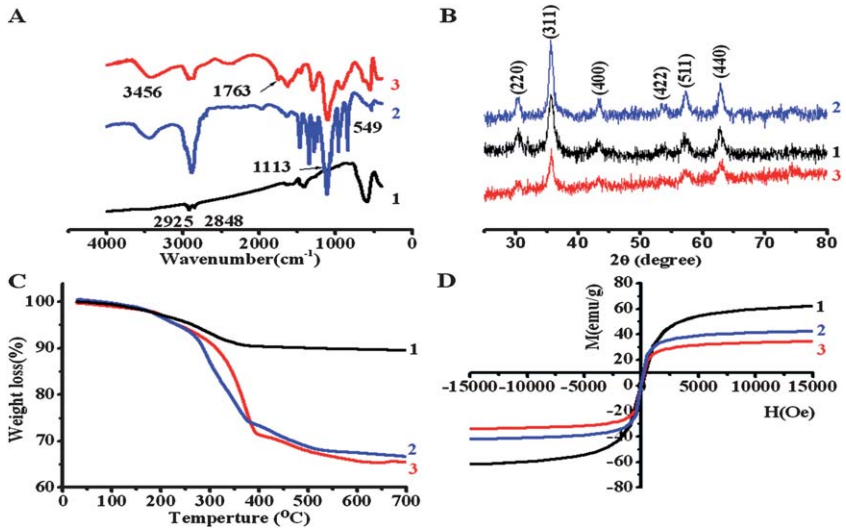

Fig. 2 (A) FT-IR spectra, (B) XRD patterns, (C) TGA curves, (D) hysteresis loops of the SPIONs (1), SPIONs @F127 (2) and SPIONs @F127–PLA (3).

phase the SPIONs, SPIONs@F127 and SPIONs@F127–PLA had *z*-average diameter values of 14.6, 29.5 and 49.3 nm, respectively, whereas in aqueous phase SPIONs@F127 and SPIONs@F127–PLA had *z*-average diameter values of 124 and 216 nm, respectively. Recently many publications have reported that F127-coated SPIONs, made using the physical adsorbing method, were well dispersed in water with the diameter about 200–400 nm,[8,27,33] which was similar to the SPIONs–F127 sample in this study (Fig. 3I). By contrast, the relatively small size of SPIONs@F127 (124 nm) could reduce nonspecific cellular uptake.

Compared with SPIONs@F127 which aggregated to form irregular clusters (Fig. 3D), SPIONs@F127–PLA spontaneously aggregated to form flower-like clusters (Fig. 3E) due to the presence of the PLA segments. When the phase transformation occurred, the structures of the magnetic nanomicelles could be

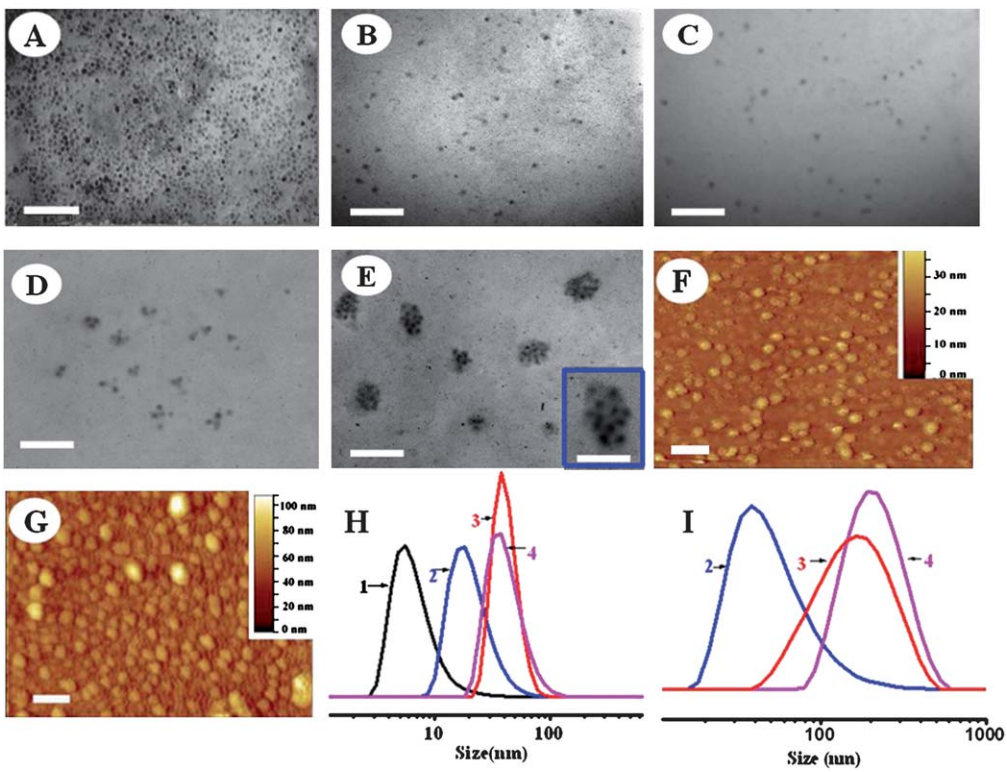

Fig. 3 TEM images of SPIONs (A), SPIONs@F127 (B), SPIONs@F127-PLA (C), dispersed in chloroform, SPIONs@F127 (D), SPIONs@F127–PLA (E), dispersed in water, AFM images of SPIONs@F127 (F), SPIONs@F127–PLA (G), dispersed in water (scale bar, 100 nm and the scale bar of inset, 50 nm), size distribution of SPIONs (1), SPIONs@F127 (2), SPIONs@F127–PLA (3) and SPIONs–F127 (4) dispersed in chloroform (H), and SPIONs@F127 (2), SPIONs@F127–PLA (3), SPIONs–F127 (4) dispersed in water (I).

tuned by the amphiphilic copolymer composition. The amphiphilic copolymer possessed the ability to assemble in solution, and the shape of the resultant nanoparticles was strongly influenced.[34–37]

3.3 Stability of the magnetic nanomicelles

The stability of the colloidal dispersion of the magnetic nanomicelles is an important parameter for biomedical applications.[38,39] In this work, the stability of the magnetic nanomicelles dispersed in the aqueous phase was studied in some specific environments. The absorbance of the magnetic nanomicelles at 350 nm (*i.e.*, the intrinsic absorption of Fe_3O_4 nanocrystals[40]) was recorded and the result illustrated in Fig. 4. Fig. 4A shows that after treatment with NaCl, both magnetic nanomicelles retained their colloidal stability which could be proved by the constant absorbance.[41] In addition, the magnetic nanomicelles were centrifuged at 5000 rpm for a set amount of time (0, 5, 10, 15, 20 min), in the case of SPIONs@F127 (Fig. 4B), no significant change was observed with an increase in centrifuging time, which suggests that SPIONs@F127 was reasonably stable under these conditions. On the other hand, the absorbance of SPIONs@F127–PLA decreased slightly.[42] Furthermore, the stability of the magnetic nanomicelles was further studied at pH 2–12 (Fig. 4C). Similarly, the absorbance of SPIONs@F127 had no significant change. By contrast, the absorbance of SPIONs@F127–PLA slightly decreased both at pH 2 and pH 12. These results indicate that the stable dispersion occurred due to the steric repulsion among the polymer chains.[43] Nevertheless, the absorbance of SPIONs@F127–PLA showed something of a decrease compared with SPIONs@F127. Both magnetic nanomicelles were well dispersed in the specific environment. That is very important in clinical applications. Recently, in the meantime, much research has been done on the colloidal stability of polymers physical adsorbed on SPIONs. Qin and co-workers pointed out that SPIONs–F127 in water showed a stable dispersion.[16] Herein, the stability of SPIONs–F127, SPIONs@F127 and SPIONs@F127–PLA dispersed in an organic phase were compared, SPIONs@F127 and SPIONs@F127–PLA dispersed in chloroform did not show any sign of deposition for about 1 month, whereas SPIONs–F127 was deposited on the bottom of the container under the same conditions (Fig. 4D).

3.4 Temperature-response of the magnetic nanomicelles

In Fig. 5A, the magnetic nanomicelles exhibited a temperature-responsive behavior. DLS results indicated that the *z*-average hydrodynamic diameter of SPIONs@F127 and SPIONs@F127–PLA decreased from 124 nm to 48 nm and from 216 nm to 141 nm, respectively, while evaluating the temperature from 25 to 45 °C. This phenomenon might be attributed to the thermo induced self-assembly of the immobilized PEO–PPO–PEO block copolymers on the SPIONs surface. While increasing the temperature, the swollen polymer chains transformed to a shrunken state corresponding to "intermolecular" and "intramolecular" hydrogen bonds, and the copolymer chains collapsed so that the copolymer shell was shrinking.[44] It is noteworthy that the *z*-average diameter of SPIONs–F127 did not change

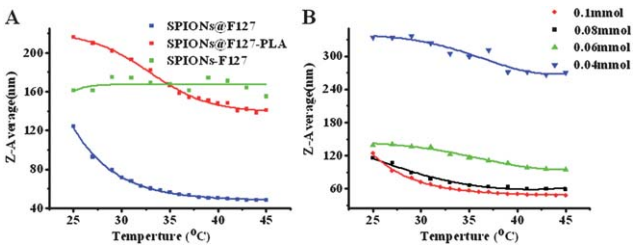

Fig. 5 Evolution of *z*-average sizes of magnetic nanomicelles dispersed in aqueous phase at different temperature with different ligands (A) and varying molar mass of the F127 (B).

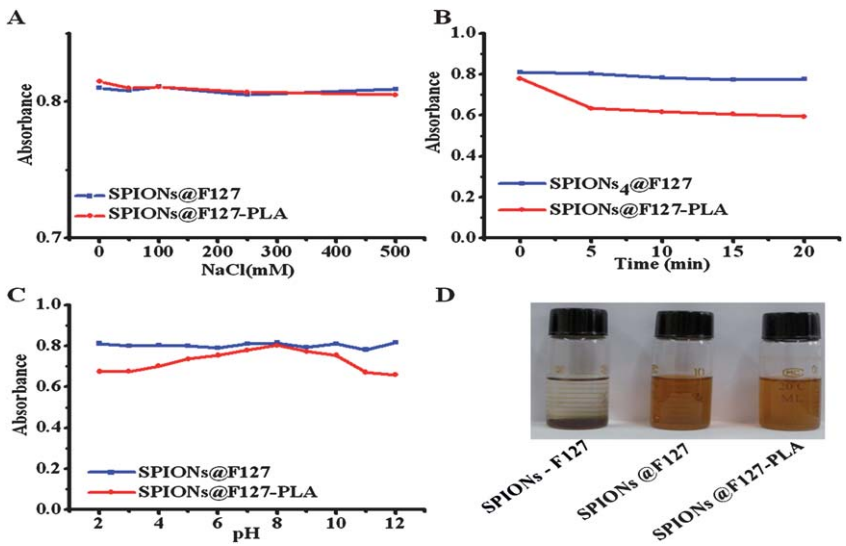

Fig. 4 Evolution of the magnetic polymer micellar absorbance dispersed in NaCl aqueous solution with various concentrations (A), centrifugal time (B) and pH values (C), the photographs (D) of SPIONs–F127 (left), SPIONs@F127 (middle) and SPIONs@F127–PLA (right) dispersed in chloroform for 1 month.

significantly. The shift region of temperature for the magnetic nanomicelles was around body temperature, which implies that they are suitable as a nanocarrier like general nanomicelles in controlled drug delivery system.

The temperature-responsive behavior of the magnetic nanomicelles affected by the synthesis parameters were investigated by DLS. Fig. 5B shows the behavior of SPIONs@F127 obtained from different molar masses of F127 ligand. At a high molar mass of F127 with high polymer surface density, the particle size was smaller than at low molar mass in the aqueous phase, meanwhile, the temperature-responsive behavior of SPIONs@F127 tends to be weakened with a decrease in the ligands molar mass. When the molar mass of F127 was decreased, the larger clusters would be formed due to interfacial balance and repulsive energy. As a result, the thermosensitivity of SPIONs@F127 tends to be weakened.

3.5 DOX·HCl loading and *in vitro* release behavior

DOX·HCl was loaded into the magnetic nanomicelles to investigate its potential application as a drug carrier. A sequential decreases in the fluorescence of DOX·HCl were observed when a fixed concentration of DOX·HCl was incubated with increasing amounts of the magnetic nanomicelles.[45] The fluorescence of DOX·HCl was quenched when the drugs were encapsulated into the magnetic nanomicelles during the drug-loading process. In Fig. 6A and B, the maximum quenching of DOX·HCl fluorescence was achieved with approximately 0.1 mg DOX·HCl to 7.137 mg SPIONs@F127 and 5.882 mg SPIONs@F127–PLA, indicating that the optimal loading amount of DOX·HCl to SPIONs@F127 and SPIONs@F127–PLA were about 1.4 wt% and 1.7 wt%, respectively.

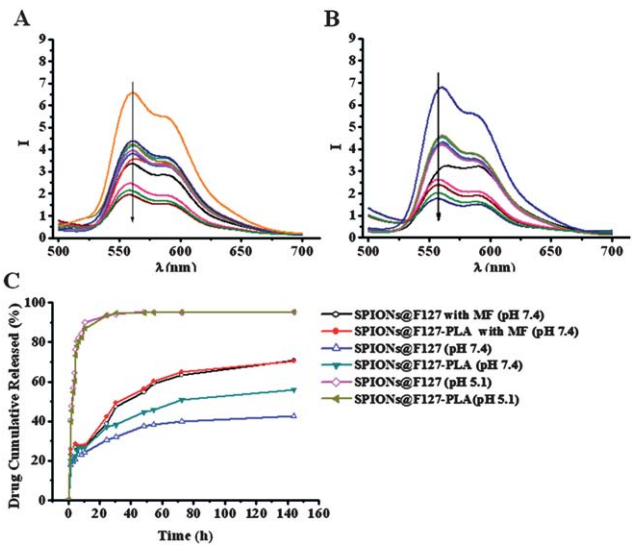

Fig. 6 Fluorescence spectra of DOX·HCl solution (0.1 mg in 3 mL of PBS solution) with increasing mass weight of SPIONs@F127 from bottom to top: 7.137, 5.037, 3.357, 1.887, 1.47, 0.891, 0.468, 0.33, 0.225, 0.200 mg (A) and SPIONs@F127–PLA with mass weight from bottom to top: 6.258, 5.882, 4.854, 2.445, 0.984, 1.089, 0.426, 0.414, 0.219, 0.198 mg (B). The release behavior of DOX·HCl over a 140 h period at different conditions (C).

SPIONs@F127–PLA could be loaded with more drugs due to its formation of bigger clusters.

The drug release kinetics were studied in specific environments (various pH values, with or without a MF). Fig. 6C shows the release behavior of DOX·HCl in PBS at pH 7.4 over 140 h under different conditions. The release profiles proved that both systems exhibited sustained release behavior at pH = 7.4 with or without a MF, but that the release rates were apparently different. The amount (55.9%) of DOX·HCl released from SPIONs@F127 without s MF within 140 h was higher than that (42.5%) from SPIONs@127–PLA, which should be attributed to the different morphologies and hydrophobic forces. Under the magnetic stimulus, the release rates increased significantly (Fig. 6C). Meanwhile, the cumulative release amount of SPIONs@F127 and SPIONs@F127–PLA reached 71.3% and 70.5% respectively. A plausible reason for this is that the encapsulation of the SPIONs within the interior of the polymer matrix brought about a magnetic response. When subjected to a MF, the SPIONs were attracted to be oriented, and the matrix was 'squeezed'. Besides, the temperature of the magnetic nanoparticles was raised induced by a MF. The reason may be that the magnetic nanoparticles could absorb energy from the MF and convert it into heat,[31,45] which might further influence the release rate of the drug. On the other hand, the release behavior of DOX·HCl proceeded much faster at pH 5.1 than at pH 7.4, which is in agreement with previous reports.[46,47,48] Upon dialysis, approximately 95.3% and 95.0% of the drug were released from the SPIONs@F127 and SPIONs@F127–PLA systems respectively within 48 h in ABS at pH 5.1. It was worth noting that the release amounts of SPIONs@F127 and SPIONs@F127–PLA were similar within 24 h. This might be due to the final concentration of DOX·HCl in the environmental solution determined by its solubility which was pH-dependent.[47]

3.6 Cytotoxicity and histochemistry analysis

HepG2 cells were incubated with the magnetic nanomicelles in Fe concentrations ranging from 10 to 25 μg mL^{-1} for various incubation times. As can be seen in Fig. 7A, the cell viabilities of SPIONs@F127 and SPIONs@F127–PLA were found to be increased further than that of SPIONs at the same concentration. However, the cell viability decreased after 3 days incubation, consisting of 80.5% and 84.3% for SPIONs@F127 and SPIONs@F127–PLA. The reason might be that the cancer cells grew too fast to get adequate space and the nutrients. Fig. 7B shows the micrographs of the HepG2 cells incubation with various magnetic nanomicelles in Fe concentrations of 25 μg mL^{-1} for 3 days. The microscopic results were consistent with those obtained from the Alamar blue assay. The morphology and the number of the cells incubated with SPIONs@F127 and SPIONs@F127–PLA were similar with the control group even at the Fe concentration 25 μg mL^{-1}, by contrast, the cells morphology became rounded and nonadherent, and the number obviously decreased when incubated with un-modified SPIONs. This indicated that the toxicity of the SPIONs would be reduced after modification with biocompatible polymers. To examine the cellular uptake of magnetic nanomicelles by HepG2 cells, Prussian blue staining was carried out. Both of samples (Fig. 7B) appeared blue due to the formation of Prussian blue precipitates

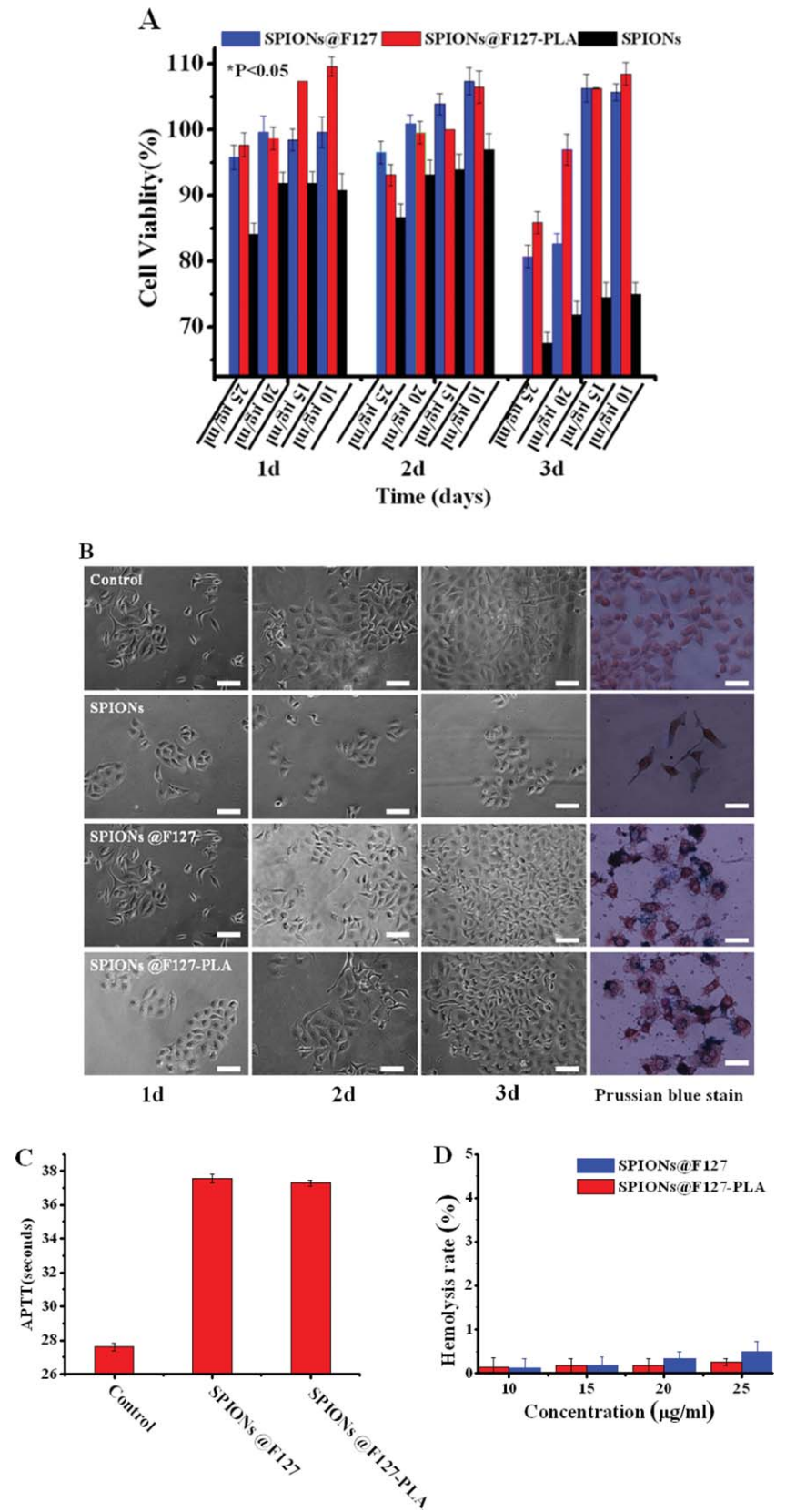

Fig. 7 The Alama blue assay of HepG2 cells growth on the different concentration of the magnetic nanomicelles (A); optical microscopic observation of HepG2 cells treated with different magnetic nanomicelles at 25 μg mL^{-1} for 3 days (scale bar, 2 μm) and Prussian blue stained of HepG2 cells after 6 h incubation with SPIONs@F127 (top) and SPIONs@F127-PLA (bottom) (scale bar, 4 μm) (B); hemolysis rate (C) and APTT analysis (D) of the magnetic nanomicelles.

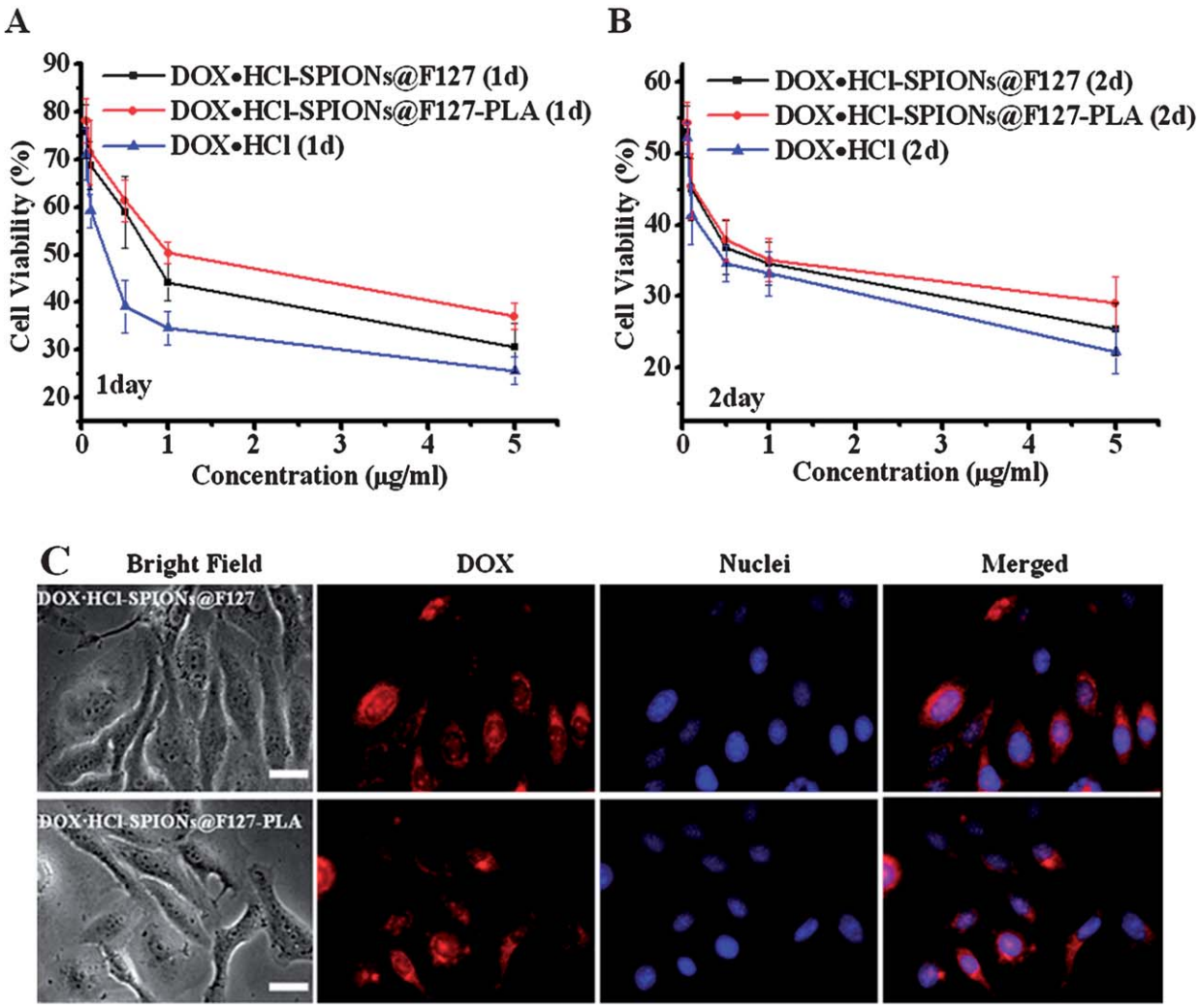

Fig. 8 Antiproliferative effect of drug in solution and loaded in magnetic nanomicelles in HepG2 cells for 1 day (A) and 2 days (B), bright-field optical image and corresponding fluorescence image of cells after 6 h incubation with DOX·HCl–SPIONs@F127 and DOX·HCl–SPIONs@F127–PLA (C) (scale bar, 8 μm). The nuclei were stained with DAPI.

inside the cells, which indicated that SPIONs@F127and SPIONs@F127–PLA were internalized into the cells by endocytosis.[41]

3.7 Blood compatibility analysis

Blood compatibility of the magnetic nanomicelles was evaluated by measuring coagulation (APTT) and hemolysis under *in vitro* conditions. Biomaterial-induced coagulation is usually initiated by the activation of intrinsic coagulation factor XII which results in kallikrein and factor XI activation.[26] The result from Fig. 7C was expressed in the seconds required for a fibrin clot to form in the plasma after the addition of the ATPP reagent. The APTT values were valid within 22–38 s, and moreover, the values of SPIONs@F127 and SPIONs@F127–PLA increased more obviously compared to the control (pure plasma). However, there was no significant difference between SPIONs@F127 and SPIONs@F127–PLA. Meanwhile, all the magnetic nanomicelles were incubated with whole blood at different concentrations (10, 15, 20, 25 μg mL^{-1}), as shown in Fig. 7D, the hemolysis rate is far less than 5% even at high concentration (25 μg mL^{-1}).

3.8 Antiproliferative effect and intracellular delivery of the DOX·HCl-loaded magnetic nanomicelles

Fig. 8A and B exhibited that both of DOX·HCl-loaded magnetic nanomicelles and free DOX·HCl had a dose-dependent antiproliferative effect on HepG2 cells over 2 days at drug concentrations of 5, 1, 0.5, 0.1 and 0.05 μg mL^{-1}. Furthermore, with increasing the drug concentration and the incubation time, the cell viability decreased. At the same drug concentration, cell viability of the cancer cells with free DOX·HCl was lower than that with DOX·HCl-loaded micelles. Additionally, the magnetic nanomicelles could decrease the toxic effect of the drug applied at high concentration, which proved the controlled and sustained efficacy of the drug release, consequently, they also would increase the maximum tolerance dose (MTD). When exposing the drug to a high concentration instantly in blood, it was presumed to be toxic not only for cancer cells but also for normal

cells.[49] We also found that the cell viability of DOX·HCl–SPIONs@F127–PLA was higher than for DOX·HCl–SPIONs@F127 during the first day, and the difference of the cell viabilities between DOX·HCl–SPIONs@F127–PLA and DOX·HCl–SPIONs@F127 was reduced after incubation for 2 days. The possible reason was this is that both DOX·HCl–SPIONs@F127–PLA and DOX·HCl–SPIONs@F127 exhibited sustained release behaviors, but the drug release rate of SPIONs@F127–PLA was slower than that of DOX·HCl–SPIONs@F127. Meanwhile, the quantity of drugs released into the body turned out to be close after the sustained release over 2 days from DOX·HCl–SPIONs@F127 and DOX·HCl–SPIONs@F127–PLA. The intracellular delivery of the DOX·HCl-loaded magnetic nanomicelles was also examined. The intrinsic fluorescence (red) of the DOX·HCl-loaded magnetic nanomicelles were observed in some areas of cells after incubation for 6 h (Fig. 8C), which demonstrated that the magnetic nanomicelles could carry and release drugs into cells following cancer cell internalization. The process of the intracellular delivery of the drug-loaded magnetic nanomicelles included the following process: firstly the drug-loaded magnetic nanomicelles were internalized *via* the endocytosis.[41,50] After being internalized into the cytoplasm, the drug-loaded magnetic nanomicelles were engulfed by endosomes.[51] Finally it accumulated in acidic lysosomes (pH 4–5) and the release rates of the pH-dependent drugs were accelerated.[52]

4. Conclusions

In this study, the multifunctional temperature-responsive and magnetic nanomicelles were successfully fabricated by using chemical conjugation method for the first time, which comprised anticancer drug, SPIONs, and temperature-responsive polymer. Those magnetic nanomicelles exhibited good aqueous stability even in some specific environments, superaramagnetism, biocompatibility and temperature-responsive properties. Meanwhile, blood compatibility studies showed that the micelles had little effect on coagulation and hemolysis. The loading and release of anticancer drug (DOX·HCl) were also investigated. It was found that the release behavior could be influenced by environmental pH vales and external magnetic fields, the *in vitro* drug release also implied that the magnetic nanomicelles could carry and release drug into the cells. As a result, we can envision that these multifunctional magnetic nanoparticles would possess many promising prospects in the application of nanomedicine.

Acknowledgements

This work was partially supported by National Natural Science Foundation of China (30970723), Programs for New Century Excellent Talents in university, Ministry of Education of China (NCET-07-0719) and Sichuan Prominent Young Talent Program (08ZQ026-040).

References

1 L. Zhang, F. X. Gu, J. M. Chan, A. Z. Wang, R. S. Langer and O. C. Farokhzad, *Clin. Pharmacol. Ther.*, 2008, **83**, 761–769.
2 J. H. Ke, J. J. Lin, J. R. Carey, J. S. Chen, C. Y. Chen and L. F. Wang, *Biomaterials*, 2010, **31**, 1707–1715.
3 H. Lee, M. K. Yu, S. Park, S. Moon, J. J. Min and Y. Y. Jeong, *J. Am. Chem. Soc.*, 2007, **129**, 12739–12745.
4 M. Lattuada and T. A. Hatton, *Langmuir*, 2007, **23**, 2158–2168.
5 N. Kohler, G. E. Fryxell and M. Q. Zhang, *J. Am. Chem. Soc.*, 2004, **126**, 7206–7211.
6 S. Laurent, D. Forge, M. Port, A. Roch, C. Robic and L. V. Elst, *Chem. Rev.*, 2008, **108**, 2064–2110.
7 K. H. Bae, S. H. Choi, S. Y. Park, Y. H. Lee and T. G. Park, *Langmuir*, 2006, **22**, 6380–6384.
8 J. Lu, S. L. Ma, J. Y. Sun, C. C. Xia, C. Liu, Z. Y. Wang, X. N. Zhao, F. B. Gao, Q. Y. Gong, B. Song, X. T. Shuai, H. Ai and Z. W. Gu, *Biomaterials*, 2009, **30**, 2919–2928.
9 D. Chen, M. Jiang, N. Li, H. Gu, Q. Xu, J. Ge, X. Xia and J. Lu, *J. Mater. Chem.*, 2010, **20**, 6422–6429.
10 P. W. Lee, S. H. Hsu, J. J. Wang, J. S. Tsai, K. J. Lin and S. P. Wey, *Biomaterials*, 2010, **31**, 1316–1324.
11 Y. Tian, P. Ravi, L. Bromberg, T. A. Hatton and K. C. Tam, *Langmuir*, 2007, **23**, 2638–2646.
12 P. Alexandridis, V. Athanassiou and T. A. Hatton, *Langmuir*, 1995, **11**, 2442–2450.
13 W. J. Duncanson, M. A. Figa, K. Hallock, S. Zalipsky, J. A. Hamilton and J. Y. Wong, *Biomaterials*, 2007, **28**, 4991–4999.
14 S. B. Zhou, X. M. Deng, W. X. Jia and L. Liu, *J. Appl. Polym. Sci.*, 2004, **91**, 1848–1856.
15 J. Sun, S. B. Zhou, P. Hou, Y. Yang, J. Weng and X. H. Li, *J. Biomed. Mater. Res. A*, 2007, **80**, 333–341.
16 J. Qin, S. Laurent, Y. S. Jo, A. Roch, M. Mikhaylova and Z. M. Bhujwalla, *Adv. Mater.*, 2007, **19**, 1874–1878.
17 J. M. Yang, T. I. Lee, J. M. Lee, E. K. Lim, W. C. Hyung and C. H. Lee, *Chem. Mater.*, 2007, **19**, 3870–3876.
18 M. K. Yu, Y. Y. Jeong, J. H. Park, S. J. Park, J. W. Kim and J. J. Min, *Angew. Chem., Int. Ed.*, 2008, **47**, 5362–5365.
19 S. J. Guo, D. Li, L. X. Zhang, J. Li and E. K. Wang, *Biomaterials*, 2009, **30**, 1881–1889.
20 A. Z. Wang, V. Bagalkot, C. C. Vasilliou, F. Gu, F. Alexis, L. F. Zhang and O. C. Farokhzad, *ChemMedChem.*, 2008, **3**, 1311–1315.
21 T. Y. Liu, S. H. Hu, K. H. Liu, R. S. Shaiu, D. M. Liu and S. Y. Chen, *Langmuir*, 2008, **24**, 13306–13311.
22 S. H. Hu, D. M. Liu, W. L. Tung, C. F. Liao and S. Y. Chen, *Adv. Funct. Mater.*, 2008, **18**, 946–955.
23 N. Blanchemain, F. Chai, M. Bacquet, L. Gengembre, M. Traisnel, Y. Setti and H. F. Hildebrand, *J. Mater. Chem.*, 2007, **17**, 4041–4049.
24 M. Martina, G. Subramanyam, J. C. Weaver, D. W. Hutmacher, D. E. Morse and S. Valiyaveettil, *Biomaterials*, 2005, **26**, 5609–5616.
25 Q. J. He, J. M. Zhang, J. L. Shi, Z. Y. Zhu, L. X. Zhang and W. B. Bu, *Biomaterials*, 2010, **31**, 1085–1092.
26 R. K. Kainthan, M. Gnanamani, M. Ganguli, T. Ghosh and D. E. Brooks, *Biomaterials*, 2006, **27**, 5377–5390.
27 Z. Zhong, Y. Zhao, Y. Koltypin and A. Gedanken, *J. Mater. Chem.*, 1998, **8**, 2167–2168.
28 J. W. Long, M. S. Logan, C. P. Rhodes, E. E. Carpenter, R. M. Stroud and D. R. Rolison, *J. Am. Chem. Soc.*, 2004, **126**, 16879–16889.
29 F. X. Hu, K. G. Neoh, L. Cen and E. T. Kang, *Biomacromolecules*, 2006, **7**, 809–816.
30 J. P. Ge, Y. X. Hu, M. Biasini, W. P. Beyermann and Y. D. Yin, *Angew. Chem., Int. Ed.*, 2007, **46**, 4342–4345.
31 C. G. Hadjipanayis, M. J. Bonder, S. Balakrishnan, X. X. Wang, H. Mao and G. C. Hadjipanayism, *Small*, 2008, **4**, 1925–1929.
32 K. El-Boubbou, D. C. Zhu, C. Vasileiou, Babak Borhan, D. Prosperi, W. Li and X. Huang, *J. Am. Chem. Soc.*, 2010, **132**, 4490–4499.
33 T. K. Jain, J. Richey, M. Strand, D. L. Leslie-Pelecky, C. A. Flask and V. Labhasetwar, *Biomaterials*, 2008, **29**, 4012–4021.
34 W. R. Zhao, H. R. Chen, Y. S. Li, L. Li, M. D. Lang and J. L. Shi, *Adv. Funct. Mater.*, 2008, **18**, 1–9.
35 Y. D. Yin and A. P. Alivisatos, *Nature*, 2005, **437**, 664–670.
36 B. G. Robert, *Nat. Mater.*, 2007, **6**, 553–555.
37 Y. Lin, S. H. kaff, T. Emrick, A. D. Dinsmore and T. P. Russell, *Science*, 2003, **299**, 226–229.
38 J. Y. Kim, H. S. Kim, N. H. Lee, T. H. Kim and T. K. Yu, *Angew. Chem., Int. Ed.*, 2008, **47**, 1–5.
39 M. Mikhaylova, D. K. Kim, N. Bobrysheva, M. Osmolowsky and V. Semenov, *Langmuir*, 2004, **20**, 2472–2477.
40 M. S. Kim, Y. F. Chen, Y. C. Liu and X. G. Peng, *Adv. Mater.*, 2005, **17**, 1429–1432.

41 J. H. Lee, K. R. Lee, S. H. Moon, Y. H. Lee, T. G. Park and J. W. Cheon, *Angew. Chem., Int. Ed.*, 2009, **48**, 4174–4179.
42 M. Kobayashi, R. Matsunob, H. Otsuka and A. Takahara, *Sci. Technol. Adv. Mater.*, 2006, **7**, 617–628.
43 L. Sun, C. Huang, T. Gong and S. B. Zhou, *Mater. Sci. Eng., C*, 2010, **30**, 583–589.
44 S. Chen, Y. Li, C. Guo, J. Wang, J. H. Ma and X. F. Liang, *Langmuir*, 2007, **23**, 12669–12676.
45 A. Shkilnyy, E. Munnier, K. Herve, M. Souce, R. Benoit, S. Cohen Jonathan, P. Limelette, M. L. Saboungi, P. Dubois and I. Chourpa, *J. Phys. Chem. C*, 2010, **114**, 5850–5858.
46 V. Bagalkot, O. C. Farokhzad, R. Langer and S. Y. Jon, *Angew. Chem., Int. Ed.*, 2006, **45**, 8149–8152.
47 L. B. Chen, F. Zhang and C. C. Wang, *Small*, 2009, **5**, 621–628.
48 B. Chang, J. Guo, C. Liu, J. Qian and W. Yang, *J. Mater. Chem.*, 2010, **20**, 9941–9947.
49 Y. T. Liu, K. Li, J. Pan, B. Liu and S. S. Feng, *Biomaterials*, 2010, **31**, 330–338.
50 Y. Zhang, M. Yang, J. H. Park, J. Singelyn, H. Ma, M. J. Sailor, E. Ruoslahti, M. Ozkan and C. Ozkan, *Small*, 2009, **5**, 1990–1996.
51 P. W. Lee, S. H. Hsu, J. J. Wang, J. S. Tsai, K. J. Lin, S. P. Wey, F. R. Chen, C. H. Lai, T. C. Yen and H. W. Sung, *Biomaterials*, 2010, **31**, 1316–1324.
52 Z. Zhou, Y. Shen, J. Tang, M. Fan, E. A. Kirk, W. J. Murdoch and Maciej Radosz, *Adv. Funct. Mater.*, 2009, **19**, 3580–3589.

